e-ISSN: 2550-164X

Available online at
https://jmeche.uitm.edu.my/

Journal of Mechanical Engineering 23(1) 2026, 63 – 83.

Journal of Mechanical Engineering

Performance Analysis of a Nonlinear Full Vehicle Model Using Double-Lane Change Maneuver: A Comparison with CarSim

Noor Amira Ilyanie Ruslan[1], Zulkiffli Abd Kadir[1*], Noor Hafizah Amer[2], Elya Mohd Nor[2]

[1]*Department of Mechanical Engineering, Faculty of Engineering, Universiti Pertahanan Nasional Malaysia, 57000, Sungai Besi, Kuala Lumpur, Malaysia*
[2]*Centre for Defence Research Technology, Universiti Pertahanan Nasional Malaysia, 57000, Sungai Besi, Kuala Lumpur, Malaysia*

ARTICLE INFO

Article history:
Received 11 August 2025
Revised 03 September 2025
Accepted 05 September 2025
Online first
Published 15 January 2026

Keywords:
Vehicle dynamics
7-DOF full vehicle model
CarSim verification
Double lane change

DOI:
10.24191/jmeche.v23i1.8460

ABSTRACT

Vehicle modelling and verification are fundamental components of the modern automotive development process, enabling researchers to optimize controller designs and ensure safety before actual testing. By employing simulation techniques, researchers can accurately predict vehicle performance and behaviour under a wide range of driving conditions. This study focuses on the development and verification of a seven-degree-of-freedom (7-DOF) full vehicle dynamics model developed to simulate real vehicle responses. The developed model consists of a handling system model, tyre dynamics model, load distribution, and individual wheel dynamics, including functions for tyre slip ratio and slip angle. The model is driven by two inputs, namely steering wheel angle and throttle position. To verify the model, its responses are compared to those generated by the CarSim software under similar vehicle parameters and driving conditions involving a double lane change maneuver at a speed of 120 km/h. The results show that the model closely follows the dynamic behaviours obtained from CarSim. The percentage difference of Root Mean Square (RMS) between the developed model and the CarSim analysis is used to evaluate the accuracy of the model. Based on the RMS values at 120 km/h, the maximum error occurred in longitudinal acceleration with a percentage difference of 5.63%. Overall, the verification results indicate that the developed model effectively tracks CarSim outputs within an acceptable range of error, demonstrating its potential for representing vehicle system dynamics under various driving conditions.

[1*] Corresponding author. *E-mail address*: zulkiffli@upnm.edu.my

https://doi.org/10.24191/jmeche.v23i1.8460

INTRODUCTION

Vehicle dynamics system focuses on analysing vehicles characteristics and responses due to external forces and input from the driver during motion. It involves understanding the complex interactions between the vehicle's subsystems, namely vehicle structure, tires, suspension system, steering system, brake system, powertrain, aerodynamics, load transfer, and the road surface (Singh & Mansour, 2023; Jin et al., 2024; Azman et al., 2025). These interactions are influenced by physical forces such as inertia, gravity, aerodynamic drag, and tire-road friction (Kojima & Raksincharoensak, 2022; Patil & Williams, 2025; Ilmi et al., 2025). The goal of vehicle dynamics model is to predict and evaluate vehicle behaviours in various driving conditions, such as during acceleration, braking, cornering, and lane changes (Wang et al., 2023; Hu et al., 2025). A well-developed vehicle dynamics system is essential for supporting virtual prototyping, reducing development costs, and accelerating innovation in vehicle automation and performance optimization. Accurate modelling of these dynamics is crucial, as it forms the foundation for designing advanced control systems, ensuring safety, and improving ride comfort (Dai et al., 2022). Models must reflect actual behaviours to be effective in simulations and control development. Without precise dynamic models, predictions may lead to unsafe or inefficient system performance.

Based on the required level of accuracy and system complexity, vehicle dynamics models are typically categorized into linear and nonlinear types. Linear models, such as the widely used two-degree-of-freedom (2-DOF) simplified bicycle model, by considering only lateral and yaw motions, assuming small slip angles, and linear tire responses (Jin et al., 2024; Yu et al., 2024). Due to their simplicity and computational efficiency, they are often employed in early-stage controller design and basic handling analysis. On the other hand, nonlinear models offer more comprehensive representations of vehicle behaviour by including additional degrees-of-freedom and complex dynamic interactions. For instance, the 7-DOF model includes longitudinal, lateral, and yaw motions, along with individual rotational dynamics of all four wheels (Li et al., 2022; Lin et al., 2024; Qiao et al., 2024). The 8 DOF model extends this by including the roll motion of the vehicle body (Wang et al., 2024). Meanwhile, the 14-DOF model consists of a 6-DOF sprung mass representing the vehicle body, which includes the longitudinal, lateral, vertical, roll, pitch, and yaw motions, and an additional 8-DOF is from the wheels, where each wheel contributes to the vertical and rotational motion, enabling high-fidelity simulation of full vehicle behaviour (Azizul et al., 2024). These nonlinear models are essential for analysing dynamic responses during aggressive maneuvers, enhancing the model's fidelity in simulations and supporting the development of reliable control strategies for modern vehicles.

To ensure the effectiveness of the vehicle dynamics model, thorough verification processes are necessary to verify that the model is correctly implemented according to its theoretical formulation and that its outputs align with actual behaviour. As models become more complex, especially in nonlinear systems with multiple degrees of freedom, the potential for inaccuracies increases which makes these processes even more critical (Cederbladh et al., 2024). On top of that, it also helps in detecting the mathematical inconsistencies or improper parameter settings that may affect the model's accuracy. Simulation tool such as CarSim is commonly used as references for model verification, as it provides high-fidelity outputs that act as a benchmark for verifying dynamic model due to its ability to replicate actual vehicle responses across various scenarios (Ataei et al., 2021). By comparing model responses with those generated in CarSim, parameters can be adjusted to ensure consistency with actual vehicle dynamics behaviour. This step is particularly crucial when the model is used for control development or performance evaluation. Therefore, verification ensures that the model is reliable, accurate and suitable for further applications in vehicle dynamics studies.

The primary objective of this study is to simulate and verify full vehicle model responses during double lane change maneuvers, offering a more realistic representation of dynamic behaviour. By including longitudinal, lateral and yaw motions along with individual wheel rotation, the model addresses the limitations in prior simplified models that often neglected critical dynamics such as slip feedback and wheel forces (Ziehn et al., 2020). The novelty of this work lies in presenting a nonlinear 7-DOF full vehicle model

https://doi.org/10.24191/jmeche.v23i1.8460

that is computationally efficient while accurately replicating the vehicle behaviour during double lane change maneuvers. This makes the model a reliable platform for validating vehicle dynamics in high-speed maneuvers while providing a foundation for the development of advanced and adaptive control strategies.

This study is structured into four main parts. The introduction presents the background on vehicle dynamics and related literature from previous researchers. Next, the modelling of the seven-degree-of-freedom (7-DOF) vehicle model discusses its development, which includes the handling dynamics, longitudinal and lateral slip characteristics, tire modelling, load distribution forces, wheel dynamics and the transformation of vehicle motion from local to global coordinates. The verification of the 7-DOF vehicle model using CarSim software outlines the procedures and analysis of the simulation results for double lane change maneuvers at a speed of 120 km/h. Finally, this study concludes with a summary of the overall work achieved.

MODELLING OF SEVEN DEGREE-OF-FREEDOMS (7-DOF) FULL VEHICLE MODEL

In this study, the developed vehicle model consists of 7-DOF, including the handling model, tyre model, effect of yaw, lateral slip angle, longitudinal slip ratio, wheel dynamics, and a kinematic model to convert the vehicle's local coordinates to global coordinates. The 7-DOF are derived from the 3-DOF of the handling model, while the remaining 4-DOF are obtained from the wheel dynamics. The model's inputs are the wheel steer angle (δ) and the engine torque (T_e). Each wheel is denoted by subscripts (i, j), where i indicates the front (f) or rear (r) wheels, and j indicates the left (l) or right (r) wheels. In the handling model, the inputs are wheel steer angle, the longitudinal force (F_{xij}) and lateral force (F_{yij}) for each tyre, while the outputs are the longitudinal acceleration (a_x), lateral acceleration (a_y) and yaw rate ($\dot{\psi}$). To model the vehicle dynamics, the effects of yaw need to be considered in generating the longitudinal velocity (V_x) and lateral velocity (V_y) of the vehicle. These velocities are used to calculate the tyre slip angle (α_{ij}) for each wheel.

Next, the tyre slip angles are then used as the input to both longitudinal slip ratio and tyre models. The longitudinal slip ratio (s_{ij}) is determined based on the vehicle's longitudinal and lateral velocities, as well as the angular velocity of each wheel (ω_{ij}). The wheel dynamics model computes the angular velocity of each wheel using the longitudinal and lateral tyre forces, as well as the applied throttling (T_{tij}) and braking torques (T_{bij}). The tyre model is then evaluated based on three vehicle dynamics inputs, namely vertical forces (F_{zij}), lateral slip angle, and longitudinal slip ratio of each wheel, where the vertical forces are obtained from a load distribution approach in which both longitudinal and lateral accelerations are set as the inputs. The overall integration of these subsystems into the full model is illustrated in Fig 1.

In this study, the overall modelling process of the 7-DOF vehicle dynamics model has been simplified through the application of several assumptions. The vehicle used in this modelling process is a front-wheel-drive type, and both the suspension and ride dynamics are excluded from the model. Although the suspension effects are neglected, the model still calculates the lateral load transfer on the tyres, which captures the dominant effect of vertical forces on vehicle handling. During maneuvering, all tyres remain in continuous contact with the ground, and the road irregularities are neglected as the vehicle is assumed to travel on a perfectly flat surface. Additionally, aerodynamic forces acting in the longitudinal direction are neglected, which allows the vehicle to move freely in both longitudinal and lateral directions as well as yaw motion around the z-axis. This simplification is justified as the focus of the model is on the lateral dynamics, where the tyre forces are dominant and are critical for assessing vehicle stability behaviour (Lugner & Plöchl, 2004). Lastly, the vehicle maintains a constant speed without braking during maneuvers while the longitudinal slip is still considered in the modelling process.

https://doi.org/10.24191/jmeche.v23i1.8460

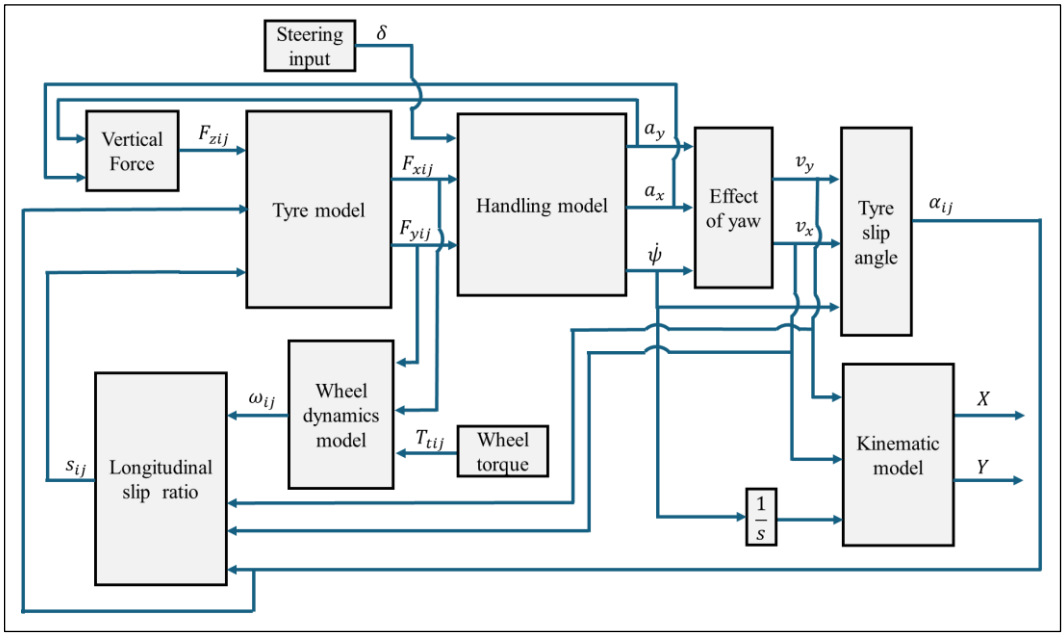

Fig. 1. The 7-DOF of the full vehicle model developed in Simulink.

Modelling of three degree-of-freedoms (3-DOF) vehicle handling model

The handling dynamics of the vehicle are represented in this study by using a 3-DOF model, which considers the motion in the longitudinal (x-direction), lateral (y-direction) and yaw (rotation about the z-axis) directions. This model is illustrated in Fig 2, also accounts for the vehicle mass (m). The effect of yaw is also included by integrating the calculated longitudinal ($\dot{v}_x$) and lateral ($\dot{v}_y$) accelerations along the x-axis and y-axis as shown in Equations 1 and 2. These equations describe the relationship between the longitudinal and lateral accelerations (a_x, a_y), velocities (v_x, v_y), and yaw rate ($\dot{\psi}$) providing a detailed representation of its dynamic behaviour.

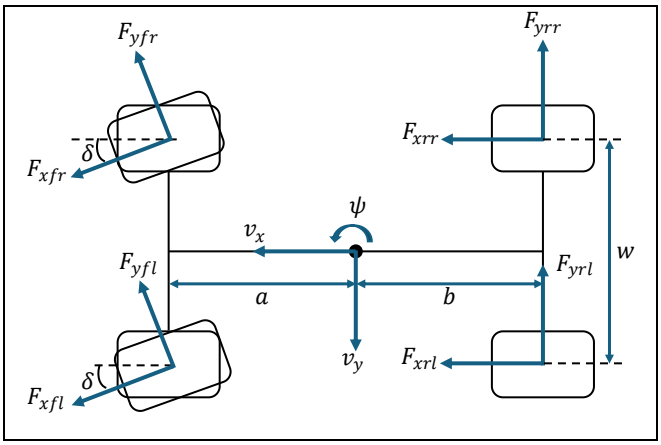

Fig. 2. A 2D diagram of the 3-DOF handling model representing vehicle motions.

https://doi.org/10.24191/jmeche.v23i1.8460

$$\dot{v}_x = a_x + v_y\dot{\psi} \tag{1}$$

$$\dot{v}_x = a_x + v_y\dot{\psi} \tag{2}$$

It is assumed that the vehicle travels on a flat road surface, with mass, m and moment of inertia about the z-axis, I_z. The vehicle width is represented by w, while a and b denote the distances from the centre of gravity (CG) to the front and rear axles, respectively. The CG is assumed to lie symmetrically between the left and right tyres, which justifies the use of the half-track width $(w/2)$ in Equation 5. The longitudinal and lateral forces acting on each wheel are denoted as F_{xij} and F_{yij}, respectively. The governing equations for the handling model in longitudinal, lateral, and yaw motions are formulated in Equations 3 to 5. These equations define the a_x, a_y and yaw angular acceleration, $\ddot{\psi}$ based on the forces acting at each wheel, which is essential in analysing the vehicle's handling dynamics.

$$a_x = \frac{F_{xfl}\cos\delta + F_{yfl}\sin\delta + F_{xfr}\cos\delta + F_{yfr}\sin\delta + F_{xrl} + F_{xrr}}{m} \tag{3}$$

$$a_y = \frac{-F_{yfl}\cos\delta + F_{xfl}\sin\delta - F_{yfr}\cos\delta + F_{xfr}\sin\delta + F_{yrl} + F_{yrr}}{m} \tag{4}$$

$$\ddot{\psi} = \frac{1}{I_z}\begin{pmatrix} \frac{w}{2}F_{xfr}\cos\delta - \frac{w}{2}F_{xfl}\cos\delta + \frac{w}{2}F_{xrr} - \frac{w}{2}F_{xrl} - \frac{w}{2}F_{yfl}\sin\delta + \\ \frac{w}{2}F_{yfr}\sin\delta + bF_{yrl} + bF_{yrr} - aF_{yfl}\cos\delta - aF_{yfr}\cos\delta \\ +aF_{xfl}\sin\delta + aF_{xfr}\sin\delta \end{pmatrix} \tag{5}$$

Modelling of longitudinal and lateral slips

In this study, the longitudinal slip ratio is determined by first calculating the longitudinal velocity components, v_{wxfj} for both the front left and right tyres using Equation 6. Here, V_{tf} and V_{tr} represents the front and left tyre speeds, and α_{fj} denotes the lateral slip angle, with subscript j indicating the left and right tyres. The front tyre speed, V_{tf} is then computed using Equation 7, which used the longitudinal and the lateral velocities, as well as the yaw angle as shown in Equation 7.

$$v_{wxfj} = V_{tf}\cos\alpha_{fj} \tag{6}$$

$$V_{tf} = \sqrt{\left(v_y + a\psi\right)^2 + v_x^2} \tag{7}$$

Similarly, the longitudinal velocity components of the rear left and right tyres, v_{wxrj} are calculated using Equation 8, while the rear tyre speed, V_{tr} is obtained using Equation 9.

$$v_{wxrj} = V_{tr}\cos\alpha_{rj} \tag{8}$$

$$V_{tr} = \sqrt{\left(v_y + b\psi\right)^2 + v_x^2} \tag{9}$$

https://doi.org/10.24191/jmeche.v23i1.8460

Once these velocity components are determined, the longitudinal slip ratio for all tyres is computed (Shahabi et al., 2021; Vošahlík & Hanis, 2024). In Equations 10 and 11, ω_{fj}, and ω_{rj} represent the angular velocities of the front and rear tyres, respectively, whereas R_w refers to the wheel radius.

$$s_{fj} = \frac{v_{wxfj} - \omega_{fj} R_w}{v_{wxfj}} \tag{10}$$

$$s_{rj} = \frac{v_{wxrj} - \omega_{rj} R_w}{v_{wxrj}} \tag{11}$$

The lateral slip angle of each tyre, α_{ij} is calculated using the vehicle's longitudinal and lateral velocities, which had been derived previously. The equations for the lateral slip angles are presented in Equations 12 to 15 (Ma et al., 2025). In this study, only front tyres are allowed to steer while the rear tyres are non-steerable, meaning $\delta_{rl} = \delta_{rr} = 0$. The derivation of the slip angle for the front left wheel is illustrated in Fig 3, where the steering angle of the front left wheel, δ_f is drawn larger than the direction of the actual wheel motion, which is represented by the arctangent term, to visually emphasize the difference between the steering input and the resulting vehicle movement. This is typical when a vehicle is cornering at higher speeds, where the tyre cannot follow the steering direction exactly due to the lateral forces. As a result, the slip angle is obtained by calculating the difference between the wheel's actual motion direction, which is expressed by the arctangent of the velocity components, and the steering angle.

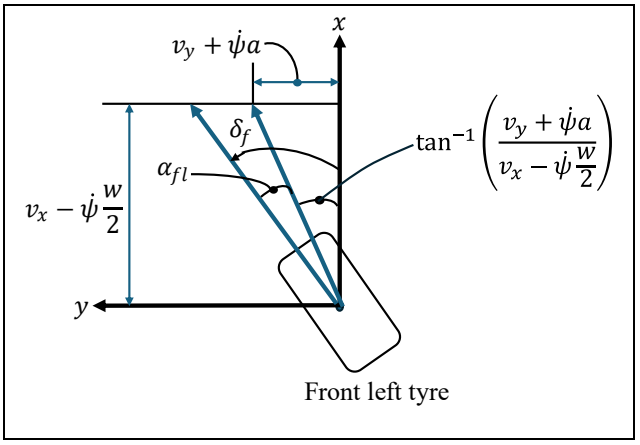

Fig. 3. Geometric-based derivation of the front-left tyre slip angle (Nam, 2015).

$$\alpha_{fl} = -\delta_{fl} + tan^{-1}\left(\frac{v_y + a\dot{\psi}}{v_x - \frac{w}{2}\dot{\psi}}\right) \tag{12}$$

$$\alpha_{fr} = -\delta_{fr} + tan^{-1}\left(\frac{v_y + a\dot{\psi}}{v_x + \frac{w}{2}\dot{\psi}}\right) \tag{13}$$

https://doi.org/10.24191/jmeche.v23i1.8460

$$\alpha_{rl} = tan^{-1}\left(\frac{v_y - b\dot{\psi}}{v_x - \frac{w}{2}\dot{\psi}}\right) \tag{14}$$

$$\alpha_{rr} = tan^{-1}\left(\frac{v_y - b\dot{\psi}}{v_x + \frac{w}{2}\dot{\psi}}\right) \tag{15}$$

Calspan tyre model

The tyre model plays a crucial role in determining the longitudinal and lateral forces generated at each wheel, which result from the interaction between the tyres and the road surface. These forces are necessary for calculating the vehicle's handling response. The Calspan tyre model is used in this study due to its ability to describe the vehicle's behaviour under various driving conditions. These include adverse driving conditions that require extreme steering, braking, acceleration, and other vehicle control maneuvers (Adnan et al., 2020). This tyre model requires three inputs, which are lateral slip angle, longitudinal slip ratio, and vertical forces of each tyre. Enhancements to the theory by Szostak et al. (1988), as refined by (Singh et al., 2000), have resulted in a more reliable definition of the saturation function, $f(\sigma)$ for generating composite forces under varying normal loads and friction coefficients. The polynomial form of this function is presented in Equation 16.

$$f(\sigma) = \frac{F_c}{\mu F_z} = \frac{C_1\sigma^3 + C_2\sigma^2 + \left(\frac{4}{\pi}\right)\sigma}{C_1\sigma^3 + C_3\sigma^2 + C_4\sigma + 1} \tag{16}$$

Here constants C_1 to C_4 are denoted as fixed parameters specific to the tyre characteristics. The tyre contact patch lengths are determined using the following equations:

$$ap_0 = \frac{0.0768\sqrt{F_z F_{ZT}}}{T_w\left(T_p + 5\right)} \tag{17}$$

$$ap = \left(1 - \frac{K_\alpha F_x}{F_z}\right) \tag{18}$$

The contact patch of tyre is represented by ap, while the tyre pressure and tread width are denoted as T_p, and T_w, respectively. Following that, F_{ZT} and K_α are represents the tyre contact patch constants. The stiffness coefficients in both lateral (K_s) and longitudinal (K_c) directions are calculated using Equations 19 and 20, where it is a function of the tyre contact patch length and normal load of the tyre.

$$K_s = \frac{2}{{ap_0}^2}\left(A_0 + A_1 F_z - \frac{A_1 {F_z}^2}{A_2}\right) \tag{19}$$

$$K_c = \frac{2}{{ap_0}^2} F_z (C_S/F_Z) \tag{20}$$

The values labeled as A_0, A_1, A_2, and C_S/F_Z are known as stiffness constants. Then, the composite slip is shown as follows:

https://doi.org/10.24191/jmeche.v23i1.8460

$$\sigma = \frac{\pi a p^2}{8\mu_0 F_z}\sqrt{{K_s}^2 tan^2\,\alpha + {K_c}^2\left(\frac{s}{1-s}\right)^2} \tag{21}$$

The nominal coefficient of friction, μ_0, varies based on road conditions, typically 0.85 is for normal roads, 0.3 for wet surfaces, and 0.1 for icy terrain. By integrating the polynomial saturation function with the lateral and longitudinal stiffness values, the overall tyre forces can be decomposed into its lateral and longitudinal forces based on the side slip angle and longitudinal slip ratio components:

$$F_y = \frac{f(\sigma)K_s\,tan\,\alpha}{\sqrt{{K_s}^2 tan^2\,\alpha + K_c' S^2}}\mu F_z \tag{22}$$

Under significant disturbances with large lateral and longitudinal forces, the sliding friction values is produced. To meet this criterion, the coefficient of friction and longitudinal stiffness coefficient are modified at high slips, as defined by K_μ.

$$K_c' = K_c + (K_s - K_c)\sqrt{sin^2\,\alpha + S^2 cos^2\,\alpha} \tag{23}$$

$$\mu = \mu_0(1 - K_\mu)\sqrt{sin^2\,\alpha + S^2 cos^2\,\alpha} \tag{24}$$

Tyre load distribution forces

In order to develop the full vehicle model, the tyre vertical force is necessary as an input for the tyre model described earlier. In this study, the vertical forces of each tyre, F_{zij} are determined using a load distribution approach during vehicle manoeuvring (Li et al., 2017). The notations used in the vertical force equations are shown in Fig 4, which considers the roll effects through the height of the gravity centre and the height of the roll centre, which influence the lateral load transfer and vertical forces. The roll angle, ϕ is assumed to be too small during manoeuvring, which allows the roll dynamics equation to be simplified while still considering the influence of roll motion. The equations consist of three main terms, where the first term represents the static load distribution when the vehicle is stationary. This term describes the vehicle's weight distribution in relation to the wheelbase, l which is the distance between the front and rear axles.

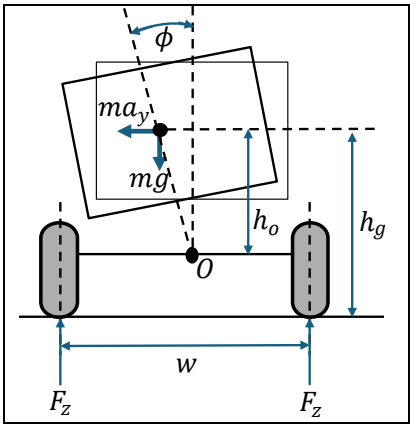

Fig. 4. Vertical load distribution model (Li et al., 2017).

https://doi.org/10.24191/jmeche.v23i1.8460

The second term describes the longitudinal load transfer caused by acceleration or deceleration, where in these equations, h_g is denoted as the height of the gravity centre. For the third term, it is dependent on the lateral acceleration and quantifies the lateral load transfer during cornering, which consists of two components, where the first component inside the brackets relates to suspension stiffness and roll centre influence. Meanwhile, the second component inside the brackets considers the effect of centre of gravity and roll centre height difference on lateral load transfer. The notations used for the third term are the height from centre of gravity to the roll centre, h_o, total roll stiffness of the suspension, K, roll stiffness of the front and rear suspensions (K_f, K_r), and the sprung mass, m_s, respectively. The vertical force equations for the front left and right wheels are written as follows:

$$F_{zfl} = \frac{b}{2l}mg - \frac{h_g}{2l}ma_x - \frac{1}{w}\left(\frac{K_f}{K - m_s g h_o} + \frac{b\left(h_g - h_o\right)}{l}\right)m_s a_y \tag{25}$$

$$F_{zfr} = \frac{b}{2l}mg - \frac{h_g}{2l}ma_x + \frac{1}{w}\left(\frac{K_f}{K - m_s g h_o} + \frac{b\left(h_g - h_o\right)}{l}\right)m_s a_y \tag{26}$$

Similarly, the vertical forces for rear left and right wheels are given in Equations 27 and 28:

$$F_{zrl} = \frac{a}{2l}mg + \frac{h_g}{2l}ma_x - \frac{1}{w}\left(\frac{K_r}{K - m_s g h_o} + \frac{a\left(h_g - h_o\right)}{l}\right)m_s a_y \tag{27}$$

$$F_{zrr} = \frac{a}{2l}mg + \frac{h_g}{2l}ma_x + \frac{1}{w}\left(\frac{K_r}{K - m_s g h_o} + \frac{a\left(h_g - h_o\right)}{l}\right)m_s a_y \tag{28}$$

Wheel dynamics model

The equations governing the rotational dynamics of the front and rear wheels are derived based on Fig 5. The equations can be expressed as follows:

$$\dot{\omega}_f = \frac{1}{I_\omega}\left(F_{xf}R_\omega - T_{bf} + T_{tf}\right) \tag{29}$$

$$\dot{\omega}_r = \frac{1}{I_\omega}\left(F_{xr}R_\omega - T_{br} + T_{tr}\right) \tag{30}$$

where the angular velocity of the front and rear wheels is represented by ω_f, and ω_r, respectively. The wheel's moment of inertia about the axle is denoted by I_ω, while R_ω refers to the wheel radius. The applied braking torques to the front and rear wheels are indicated by T_{bf}, T_{br}, whereas T_{tf}, T_{tr}, represents the throttling torques for the respective wheels.

https://doi.org/10.24191/jmeche.v23i1.8460

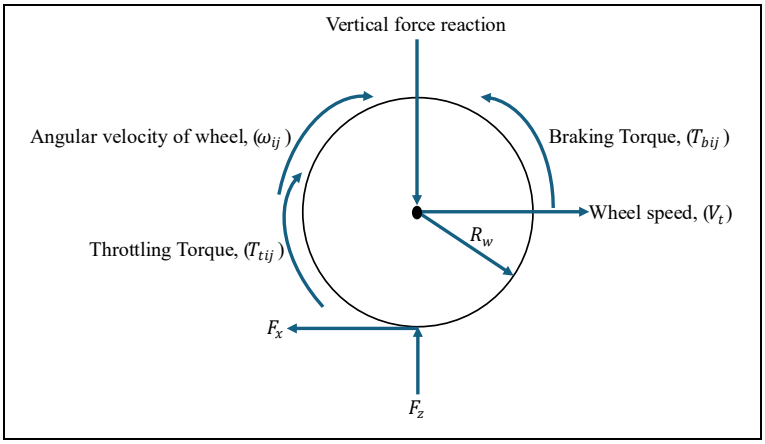

Fig. 5. Free body diagram of a wheel (Ahmad et al., 2010).

Meanwhile, it is essential to calculate the throttling torques in terms of engine characteristics and drivetrain parameters to obtain the angular velocity of the wheels. The throttling torque applied to the front and rear wheels, T_{tf} and T_{tr}, is expressed as follows:

$$T_{tf} = T_{emax} \times GR_f \times Throttle\ Position \tag{31}$$

$$T_{tr} = T_{emax} \times GR_r \times Throttle\ Position \tag{32}$$

where the maximum engine torque is denoted as T_{emax}, the transmission gear ratios for the front and rear wheels are represented by GR_f, and GR_r respectively, and the throttle position is from the driver's input. By substituting the throttling torques into Equations 31 and 32, the wheel's rotational dynamics can be described by connecting the powertrain inputs, such as the throttle position and gear ratio, to the angular acceleration of the wheels. Since the angular acceleration affects the wheel's tangential velocity, this relationship is important in understanding the vehicle's overall motion and traction behaviour (Widner et al., 2022). In the context of a front-wheel-drive (FWD) vehicle configuration, only the front wheels are mechanically linked to the powertrain. Therefore, the rear wheels do not receive any engine torque, and the corresponding throttling torque simplifies to $T_r = 0$.

Kinematic model of global coordinates

The kinematic model plays a crucial role in trajectory control strategies. It is commonly used to transform the vehicle's position from local coordinates to global coordinates, enabling the observation of vehicle movement along an actual path, as shown in Fig 6.

The vehicle's velocity in global coordinates is obtained by resolving its velocity components from the local coordinate (x-y) into the global coordinate system, as expressed in Equations 33 and 34, where ψ is the yaw angle.

$$v_X = v_x \cos\psi - v_y \sin\psi \tag{33}$$

$$v_Y = v_x \sin\psi + v_y \cos\psi \tag{34}$$

https://doi.org/10.24191/jmeche.v23i1.8460

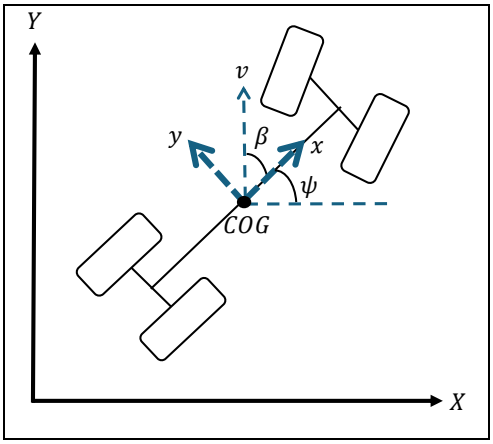

Fig. 6. Vehicle's position in global coordinate.

The vehicle's displacement in the global coordinate is then determined by integrating Equations 33 and 34 as formulated in Equations 35 and 36 (Zhang et al., 2024). This model is applied when all sub-models are combined to produce longitudinal acceleration, lateral acceleration, and yaw motions, which are then used as inputs for this kinematic model to obtain global coordinates.

$$X = \int_0^t \left(v_x \cos\psi - v_y \sin\psi\right) dt \tag{35}$$

$$Y = \int_0^t \left(v_x \sin\psi + v_y \cos\psi\right) dt \tag{36}$$

VERIFICATION OF 7-DOF VEHICLE MODEL DUE TO STEERING WHEEL INPUTS

In this section, the derived equations of the full 7-DOF vehicle model are verified using CarSim software. The verification process involves a double lane change maneuver performed at a speed of 120 km/h to evaluate the developed vehicle model responses. This speed was chosen because it represents the upper legal highway limit in Malaysia, which allows the study to capture worst-case dynamics during DLC maneuvers. Although verification at multiple speeds can be informative, this study focuses on high-speed performance as the most critical safety scenario. Some parameters used in the developed vehicle model are obtained from previous studies and are applied in the CarSim software to get similar types of vehicle specifications. This section provides a detailed explanation of the CarSim setup, verification procedures, and analysis of the responses between the developed 7-DOF model with CarSim responses.

Verification and setup procedures of Carsim software

For the verification process, the CarSim 2012 software is used to simulate and analyze vehicle performance under various driving conditions. This software is widely recognized for its ability to provide detailed vehicle handling characteristics and behaviors by representing the actual vehicle systems. CarSim enables users to define specific vehicle parameters, driving maneuvers, and environmental conditions to predict vehicle behavior accurately. This section presents the setup and configuration of the software used in this study. The type of vehicle used in this study is a sedan vehicle, where the vehicle parameters are configured by setting several parameters, such as mass, inertia properties, and dimensions of the vehicle,

https://doi.org/10.24191/jmeche.v23i1.8460

to represent the actual vehicle. Once the vehicle configuration is set, the maneuver selection begins. This step involves specifying the driving conditions under which the vehicle will be tested. The maneuver setup includes speed settings and environmental factors such as road surface conditions. The overall process of setting up the vehicle model, configuring parameters, and defining the maneuver is illustrated in Fig 7.

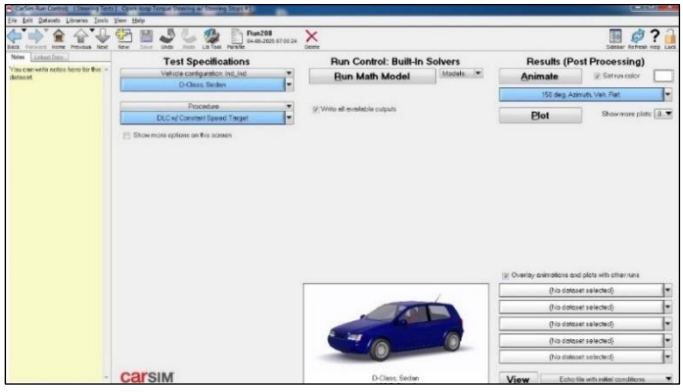

(a)

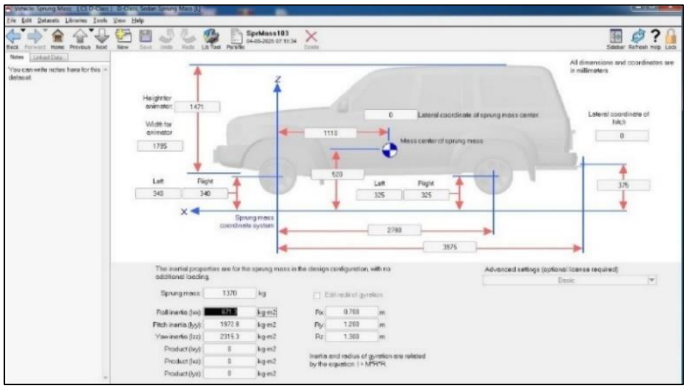

(b)

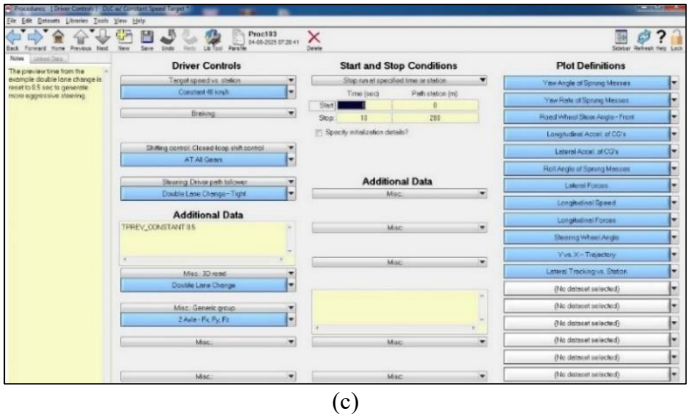

(c)

Fig. 7. Procedure setup and maneuver selection in CarSim: (a) vehicle selection and initial setup, (b) vehicle parameters configuration and (c) maneuver setup and speed configuration.

https://doi.org/10.24191/jmeche.v23i1.8460

The targeted path for the double lane change maneuver is shown in Fig 8. The vehicle initially follows a straight path for the first 90 meters before executing the first lane change. It then maintains a straight trajectory for approximately 70 meters before performing the second lane change, followed by another 70 meters of straight-line travel. This maneuver is tested at a speed of 120 km/h.

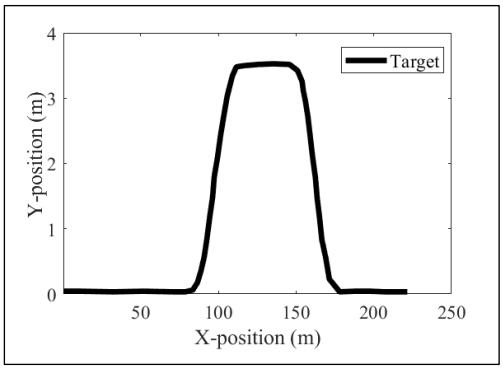

Fig. 8. Targeted path for double lane change maneuver in CarSim (Zhang et al., 2023).

Selected vehicle parameters, such as mass, inertia, and dimensions, as tabulated in Table 1, are applied in the Simulink-based 7-DOF vehicle model to ensure consistency with the setup configured in CarSim. These parameters are based on a standard sedan configuration. The exact specifications may vary across different sedan models; the chosen values follow the CarSim setup and fall within the expected range for the passenger sedans. This ensures that the model represents the sedan type of passenger vehicles. Meanwhile, the tyre model parameters used in Simulink are based on a previous study under normal road conditions, as shown in Table 2, where the tyre characteristics have been verified for use in the double lane change simulations (Abdullah et al., 2021).

Verification results for double lane change test at 120 km/h

This section discusses the verification results of the developed vehicle model in Simulink by comparing its output responses with the responses obtained in the CarSim software. For the simulation, the duration is set to be 10 seconds using a fixed-step solver (ode3, Bogacki-Shampine solver) with a step size of 0.01 for a speed of 120 km/h. To evaluate the model's accuracy, the percentage difference of the Root Mean Square (RMS) between the responses from Simulink and CarSim is calculated. The results for all responses are shown in Fig 9 to Fig 16. In these figures, black solid lines represent the outputs of the developed model, while grey solid lines denote the outputs from CarSim.

Table 1. Simulation parameters for the vehicle model

Parameters	Value
m	1530 kg
I_z	2315.3 kg.m^2
a	1.11 m
b	1.67 m
w	1.55 m
h_o	0.195 m

https://doi.org/10.24191/jmeche.v23i1.8460

Table 2. Parameters of the tyre

Parameters	FWD radial
Tyre designation	P185/70 R13
T_w	7.3
T_p	24
F_{ZT}	980
C_1	1.0
C_2	0.34
C_3	0.57
C_4	0.32
A_0	1068
A_1	11.3
A_2	2442.73
A_3	0.31
A_4	-1877
K_α	0.05
CS/FZ	17.91
μ_0	0.85

In order to verify the developed model, the vehicle's longitudinal, lateral, and yaw motions as well as its global coordinates are evaluated. Based on Fig 9, the longitudinal acceleration responses of the developed model for speed 120 km/h are closely aligned with the CarSim response. However, minor deviations are observed and quantified using the percentage difference of the RMS values. At 120 km/h, the RMS value for the developed model is 0.5702 m/s², while the CarSim RMS value is 0.5398 m/s², resulting in a percentage difference of 5.63%.

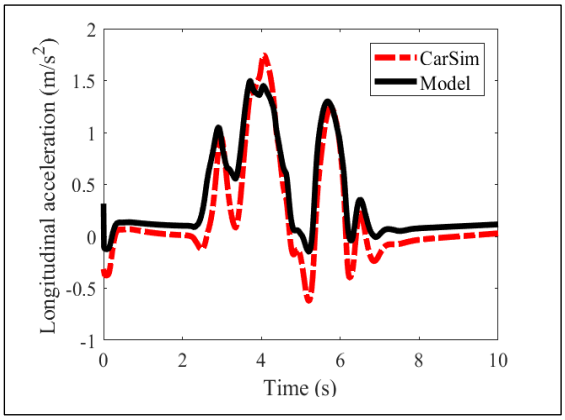

Fig. 9. Response of longitudinal acceleration during a double lane change maneuver at a speed of 120 km/h.

The next assessment in the verification process focuses on longitudinal velocity. As illustrated in Fig 10, the developed model shows minor deviations in longitudinal velocity when compared to the CarSim response at 120 km/h. In CarSim, the throttle input is adjusted automatically to follow the double lane change path. This results in a smoother and more stable velocity profile compared to the developed model response. Since the developed model does not include an automatic throttle control to maintain constant speed, it results in consistent magnitude fluctuations in velocity during the maneuvering. Despite these fluctuations, the overall longitudinal velocity trend of the developed model still aligns with the CarSim

https://doi.org/10.24191/jmeche.v23i1.8460

results. This is further supported by the RMS analysis, where the model and CarSim recorded RMS values of 34.0347 m/s and 33.3247 m/s, respectively, which results in a percentage difference of 2.13%. This relatively low deviation demonstrates the model's ability to accurately simulate the vehicle's longitudinal velocity response during high-speed double lane change maneuvers, even without an automatic throttle control system.

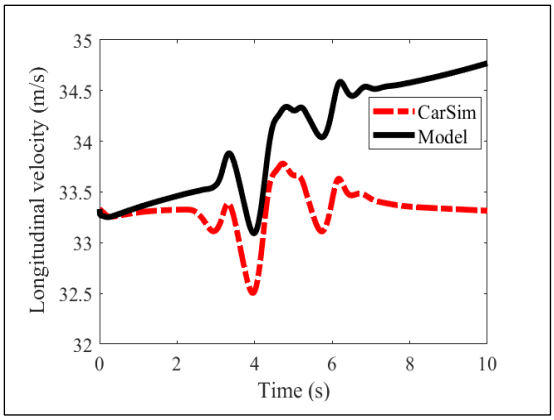

Fig. 10. Response of longitudinal velocity during a double lane change maneuver at a speed of 120 km/h.

Fig 11 shows the lateral acceleration responses for the double lane change at 120 km/h. The model managed to track the CarSim response well with slight deviations observed between 4.5 seconds to 5.0 seconds and also occurred at 7.0 seconds. These deviations are due to differences in the magnitude of the longitudinal and lateral tire forces in the model, particularly at the rear tires, which indicate the higher magnitude deviations at 120 km/h. Mathematically, both longitudinal and lateral accelerations are influenced by longitudinal forces (F_{xij}), lateral forces (F_{yij}), steering angle (δ), and vehicle mass (m). At higher speeds, the deviations in these forces become larger, contributing to the observed differences. For lateral acceleration, the RMS value for the model is 3.5186 m/s², while the CarSim value is 3.5807 m/s², resulting in a percentage difference of 1.73%, which falls well within 0% to 15% range generally accepted for RMS error in model verification (Adnan et al., 2020; Azizul et al., 2024), demonstrating the model's reliability under dynamic conditions.

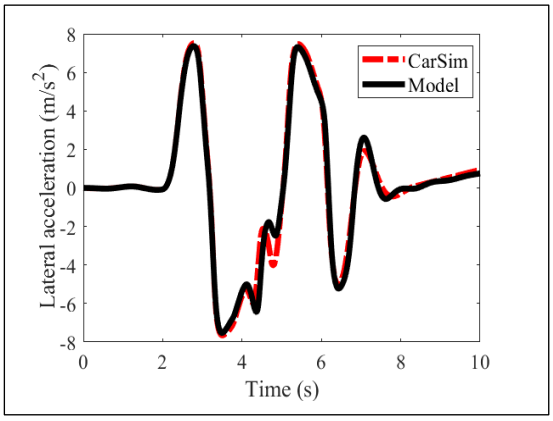

Fig. 11. Response of lateral acceleration during a double lane change maneuver at a speed of 120 km/h.

https://doi.org/10.24191/jmeche.v23i1.8460

Fig 12 represents the verification results for lateral velocity during the double lane change maneuver at 120 km/h. The developed model closely follows the CarSim trend, with minor deviations observed during the maneuver. These minor deviations observed are primarily due to variations in the calculated lateral acceleration, which are influenced by the tire's longitudinal and lateral forces. Additionally, the lateral velocity response is not only affected by lateral tire forces and steering angle input but also by the feedback of the longitudinal velocity. The RMS values obtained for the developed model and CarSim are 2.3810 m/s and 2.2564 m/s, respectively, with a percentage difference of 5.52% for a speed of 120 km/h.

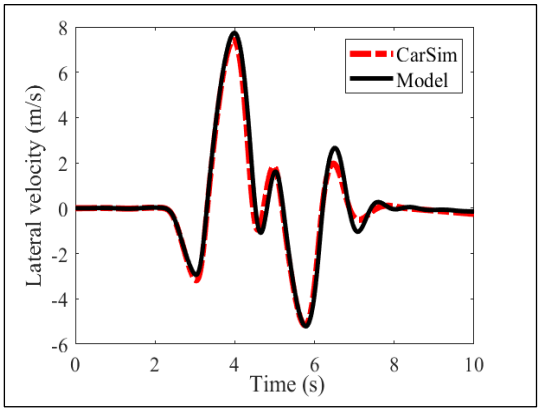

Fig. 12. Response of lateral velocity during a double lane change maneuver at a speed of 120 km/h.

For the yaw angular acceleration responses as shown in Fig 13, a slight deviation is observed at 120 km/h beginning at 4 seconds. These differences are because of the combined effects of longitudinal and lateral forces, steering input, and the vehicle's moment of inertia, which influence the characteristics of the yaw angular acceleration. To analyse the deviations, the percentage difference of RMS values is calculated, showing the deviation of 2.40% at 120 km/h, where the RMS values are 0.0213 rad/s² for the developed model and 0.0208 rad/s² for CarSim response.

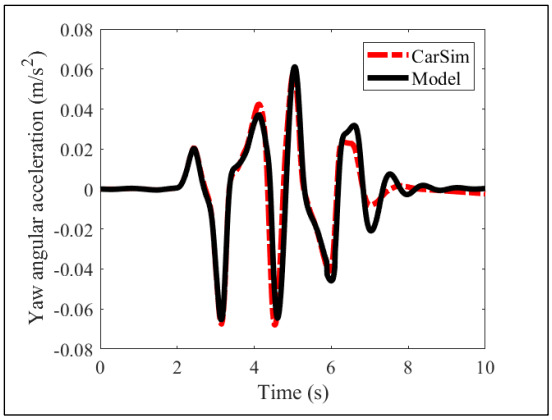

Fig. 13. Response of yaw angular acceleration during a double lane change maneuver at a speed of 120 km/h.

For the yaw rate response as presented in Fig 14, for 120 km/h, the model is able to closely follow the CarSim response. The deviations observed are due to the difficulties of vehicle models in accurately following the targeted path at higher speeds. Even though there are deviations, the model still manages to

https://doi.org/10.24191/jmeche.v23i1.8460

track the CarSim yaw rate trend effectively. The percentage difference of RMS values obtained between the developed model and CarSim for yaw rate is 1.38%, with respective RMS values of 0.2646 rad/s and 0.2683 rad/s, indicating a small deviation.

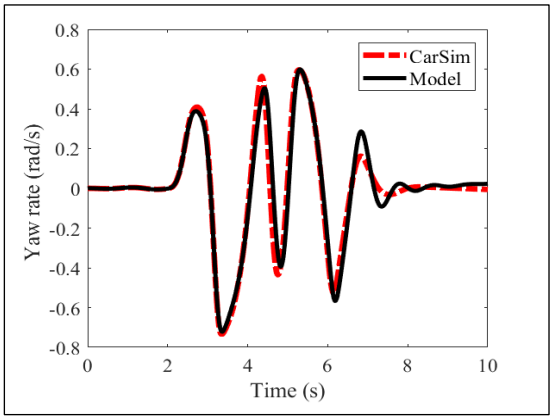

Fig. 14. Response of yaw rate during a double lane change maneuver at a speed of 120 km/h.

Lastly, the yaw angle response is analyzed for a speed of 120 km/h, as illustrated in Fig 15 shows a close match between the developed model and the CarSim response. The yaw angle was obtained by applying double integration to the yaw rate response. The root mean square (RMS) value of the yaw angle from the developed model is 0.0949 rad, compared to 0.0904 rad from CarSim. This results in a percentage difference of 4.98%, indicating that the model is capable of accurately capturing the yaw behavior, even at high speed.

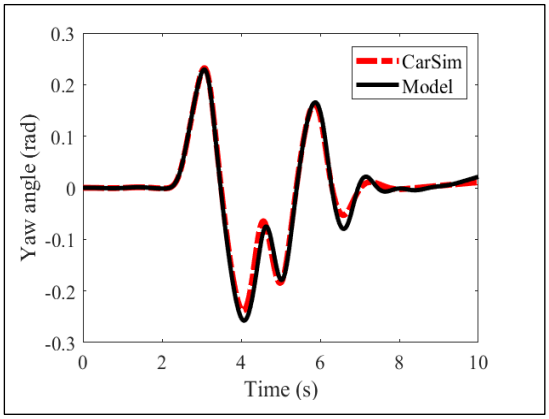

Fig. 15. Response of yaw angle during a double lane change maneuver at a speed of 120 km/h.

In order to evaluate the tracking accuracy, the vehicle's actual position during the double lane change test represented by global *X*-*Y* coordinates is analysed by comparing the model with the CarSim responses as shown in Fig 16. Although the targeted path is shown in the figure for visual reference, the quantitative comparison focuses mainly on the trajectories of the Simulink model and Carsim. At 120 km/h, the RMS value for the *X*-coordinate is 195.4695 m for the model and 192.5388 m for CarSim, resulting in a percentage RMS difference of 1.52%. For the Y-coordinate, the RMS value is 1.5316 m for the model and

https://doi.org/10.24191/jmeche.v23i1.8460

1.4782 m for CarSim, corresponding to a 3.61% RMS difference. The increased deviation at 120 km/h is primarily due to the vehicle model's reduced ability to accurately follow the intended path. At higher speeds, the vehicle travels a greater distance in a shorter time, allowing less time to react to steering inputs and perform lane changes. Furthermore, sharper turning at 120 km/h induces greater lateral forces, which can reduce tire grip, increase slip angles, and elevate the risk of understeer or oversteer. These results indicate that the developed vehicle model shows slightly reduced accuracy in tracking the CarSim trajectory at higher speeds, particularly in lateral movement along the *Y*-axis.

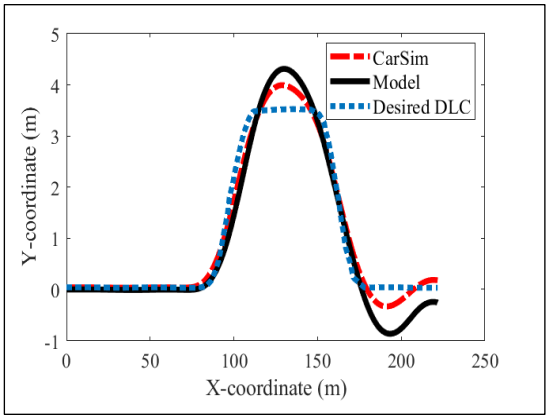

Fig. 16. Response of *X*-*Y* coordinates during a double lane change maneuver at a speed of 120 km/h.

CONCLUSION

The study had developed a 7-DOF vehicle dynamics model that consists of handling dynamics, tire slip models, wheel dynamics, and a kinematic model to realistically simulate vehicle motion. The model consists of 3-DOF for vehicle longitudinal, lateral, and yaw motions, as well as 4-DOF for the wheel rotational dynamics, for each wheel. Several assumptions were made to simplify the model, allowing for a more efficient and manageable analysis. These include assuming the vehicle body is rigid without suspension articulation, using symmetrical geometry, and maintaining constant mass and inertia throughout the simulation. Additionally, the model excludes aerodynamic forces, road gradient effects, drivetrain losses, and brake dynamics, and it employs the Calspan tire model under the assumption of uniform and ideal road conditions. The model was verified through a double lane change maneuver at 120 km/h. Based on the verification results, the percentage difference of the RMS values between the developed model and CarSim responses was calculated. The results indicate that the developed model showed similar trends to those produced by CarSim, with all percentage errors below 15% which is considered acceptable. The observed deviations are due to the simplification of the mathematical model, which does not consider all dynamic characteristics present in the CarSim simulation. These simplifications, along with certain assumptions and neglected factors, contribute to the differences between the model and CarSim responses. Overall, the minor deviations indicate that the developed vehicle model is capable of accurately representing vehicle behavior during a double lane change, closely following the trends generated by CarSim. This model also provides a computationally efficient platform for vehicle dynamics analysis, controller development, and handling and safety assessment for passenger vehicles. The limitation found in this study includes testing at a single speed, idealized road and tyre conditions, and the exclusion of suspension, aerodynamic, and brake dynamics. Therefore, future work could extend the model verification

https://doi.org/10.24191/jmeche.v23i1.8460

by testing with multiple speeds, considering environmental and vehicle factors, and evaluating additional maneuvers to further enhance its overall relevance and impact.

ACKNOWLEDGEMENT

The authors would like to thank the Ministry of Higher Education (MOHE) Malaysia, for the financial support through the Fundamental Research Grant Scheme: (FRGS/1/2024/TK10/UPNM/02/4) and Universiti Pertahanan Nasional Malaysia (UPNM) for providing the research facilities used in this study.

CONFLICT OF INTEREST STATEMENT

The authors declare that they have no conflict of interest.

AUTHORS' CONTRIBUTIONS

The authors confirm their contribution to the paper as follows: developed the 7-DOF vehicle dynamics model, designed the simulation framework and draft manuscript preparation: Noor Amira Ilyanie Ruslan; provided supervision, validation procedures and manuscript review: Zulkiffli Abd Kadir; performed the CarSim simulations and conducted RMS error analysis: Noor Amira Ilyanie Ruslan, Zulkiffli Abd Kadir; integration of the Simplified Calspan tire model and refinement of the vehicle dynamic equations: Noor Hafizah Amer, Elya Mohd Nor. All authors reviewed the results and approved the final version of the manuscript.

REFERENCE

Abdullah, M. A., Harun, M. H., Ahmad, F., Singh, A. S. P., & Mohan, A. E. (2021). Tire model verification and performance comparison using double lane change test. Journal of Mechanical Engineering and Technology, 13(1), 25–59.

Adnan, M. N. H., Kadir, Z. A., Amer, N. H., Hudha, K., Yussof, M. A. M., & Aparow, V. R. (2020). Development and verification of a 3-DOF trailer model for truck vehicles. 16th IEEE International Colloquium on Signal Processing & Its Applications (pp. 120–125). IEEE Publisher.

Ahmad, F., Hudha, K., Imaduddin, F., & Jamaluddin, H. (2010). Modelling, validation and adaptive PID control with pitch moment rejection of active suspension system for reducing unwanted vehicle motion in longitudinal direction. International Journal of Vehicle Systems Modelling and Testing, 5(4), 312-346.

Ataei, M., Khajepour, A., & Jeon, S. (2021). Development of a novel general reconfigurable vehicle dynamics model. Mechanism and Machine Theory, 156, 104147.

Azizul, M. A., Ahmad, F., Karjanto, J., Che Hasan, M. H., & Sulaiman, S. (2024). Modelling, simulation and testing of steer-by-wire system with variable steering ratio control strategy in 14-DOF full vehicle model. International Journal of Automotive and Mechanical Engineering, 21(4), 11784–11808.

Azman, A. N. N., Venkatason, K., & Sivaguru, S. (2025). Mathematical modelling of sedan vehicle front-

end profiles for aerodynamics efficiency analysis. Journal of Mechanical Engineering, 22(2), 173–189.

Cederbladh, J., Cicchetti, A., & Suryadevara, J. (2024). Early validation and verification of system behaviour in model-based systems engineering: a systematic literature review. ACM Transactions on Software Engineering and Methodology, 33(3), 81.

Dai, W., Pan, Y., Min, C., Zhang, S. P., & Zhao, J. (2022). Real-time modeling of vehicle's longitudinal-vertical dynamics in ADAS applications. Actuators, 11(12), 378.

Hu, J., Liu, H., Yi, S., & Huang, C. (2025). Lane-changing control strategy for distributed drive vehicles considering yaw stability. IET Intelligent Transport Systems, 19(1), e12605.

Ilmi, I., Adhitya, M., & Rawikara, S. S. (2025). Vehicle model development for energy consumption study: for diesel mining truck. Journal of Mechanical Engineering, 22(1), 154–175.

Jin, L., Zhao, S., & Xu, N. (2024). A survey of vehicle dynamics models for autonomous driving. WCX SAE World Congress Experience (pp. 1-13). SAE International.

Kojima, T., & Raksincharoensak, P. (2022). Environment-on-board predictive braking control functions for autonomous driving during sudden changes in the road friction coefficient on sharp curves. International Journal of Automotive Technology, 23(2), 451–460.

Li, L., Lu, Y., Wang, R., & Chen, J. (2017). A three-dimensional dynamics control framework of vehicle lateral stability and rollover prevention via active braking with MPC. IEEE Transactions on Industrial Electronics, 64(4), 3389–3401.

Li, R., Yu, Y., Sun, Y., Lu, Z., & Tian, G. (2022). Trajectory following control for automated drifting of 4WID vehicles. WCX SAE World Congress Experience (pp. 1-12). SAE International.

Lin, F., Wang, X., Qian, C., Zhao, Y., & Wu, J. (2024). Coordinated longitudinal and lateral motion control for distributed drive electric vehicles with mechanical elastic wheels. IEEE Transactions on Transportation Electrification, 10(1), 523–539.

Lugner, P., & Plöchl, M. (2004). Modelling in vehicle dynamics of automobiles. Journal of Applied Mathematics and Mechanics, 84(4), 219–236.

Ma, Y. J., Chen, C. K., & Ren, H. (2025). Research on lateral stability control of four-wheel independent drive electric vehicle based on state estimation. Sensors, 25(2), 474.

Nam, K. (2015). Application of novel lateral tire force sensors to vehicle parameter estimation of electric vehicles. Sensors, 15(11), 28385–28401.

Patil, H., & Williams, D. (2025). Aerodynamic effect on vehicle handling. WCX SAE World Congress Experience (pp. 1-12). SAE International.

Qiao, Y., Chen, X., & Yin, D. (2024). Coordinated control for the trajectory tracking of four-wheel independent drive–four-wheel independent steering electric vehicles based on the extension dynamic stability domain. Actuators, 13(2), 77.

Shahabi, A., Kazemian, A. H., Farahat, S., & Sarhaddi, F. (2021). Wheel slip ratio regulation for investigating the vehicle's dynamic behavior during braking and steering input. Mechanics and Industry, 22, 1-11.

Singh, S., & Mansour, I. (2023). Design evolution of vehicle dynamics and controls from mechanization,

https://doi.org/10.24191/jmeche.v23i1.8460

electrification to autonomy. WCX SAE World Congress Experience (pp. 1-15). SAE International.

Singh, T., Kesavadas, T., Mayne, R., Kim, J. J., & Roy, A. (2000). Design of hardware/algorithms for enhancement of driver-vehicle performance in inclement conditions using a virtual environment. Journal of Passenger Cars: Mechanical System Journal, 109, 432–443.

Szostak, H. T., Allen, W. R., & Rosenthal, T. J. (1988). Analytical modeling of driver response in crash avoidance maneuvering volume II: an interactive model for driver/vehicle simulation. University of Michigan Transportation Research Institute.

Vošahlík, D., & Hanis, T. (2024). Real-time estimation of the optimal longitudinal slip ratio for attaining the maximum traction force. Control Engineering Practice, 145, 105876.

Wang, W., Qu, F., Guo, C., & Li, W. (2023). Research on the trajectory tracking of a curved road in an active lane change scenario based on model predictive control algorithm. Advances in Mechanical Engineering, 15(9), 1-20.

Wang, Y., Lian, R., He, H., Betz, J., & Wei, H. (2024). Auto-tuning dynamics parameters of intelligent electric vehicles via Bayesian optimization. IEEE Transactions on Transportation Electrification, 10(3), 6915-6927.

Widner, A., Tihanyi, V., & Tettamanti, T. (2022). Framework for vehicle dynamics model validation. IEEE Access, 10, 35422–35436.

Yu, Z., Zhao, R., & Yuan, T. (2024). Lateral-stability-oriented path-tracking control design for four-wheel independent drive autonomous vehicles with tire dynamic characteristics under extreme conditions. World Electric Vehicle Journal, 15(10), 465.

Zhang, S., Liu, X., Deng, G., Ou, J., Yang, E., Yang, S., & Li, T. (2023). Longitudinal and lateral control strategies for automatic lane change to avoid collision in vehicle high-speed driving. Sensors, 23(11), 5301.

Zhang, T., Sun, Y., Wang, Y., Li, B., Tian, Y., & Wang, F. Y. (2024). A survey of vehicle dynamics modeling methods for autonomous racing: theoretical models, physical/virtual platforms, and perspectives. IEEE Transactions on Intelligent Vehicles, 9(3), 4312–4334.

Ziehn, J. R., Ruf, M., Roschani, M., & Beyerer, J. (2020). Accuracy evaluation of a lightweight analytic vehicle dynamics model for maneuver planning. 5th International Conference on Robotics and Automation Engineering (pp. 197–205). IEEE Publisher.

https://doi.org/10.24191/jmeche.v23i1.8460